Perpendicular effective field induced by spin-orbit torque and magnetization damping in chiral domain walls

Tie Zhou,[1,*] Sai Zhou,[2,*] Xuejie Xie,[1] Xiaonan Zhao,[1] Yanan Dong,[1] Jing Wang,[1] Weibin Chen,[1,3] Qunwen Leng,[3] Lihui Bai,[1] Yanxue Chen,[1] Shishou Kang,[1] Yaowen Liu,[2] Shishen Yan,[1,†] and Yufeng Tian[1,‡]

[1]*School of Physics, State Key Laboratory of Crystal Materials, Shandong University, Jinan 250100, People's Republic of China*
[2]*School of Physics Science and Engineering, Tongji University, Shanghai 200092, People's Republic of China*
[3]*Beihang University, Beihang Goertek Joint Microelectronics Institute, Qingdao Research Institute, Qingdao 266101, People's Republic of China*

(Received 19 December 2021; revised 17 January 2023; accepted 1 March 2023; published 13 March 2023)

The effective magnetic fields induced by spin-orbit torque (SOT), Dzyaloshinsky-Moriya exchange interaction, and magnetization damping in chiral domain wall systems are very important to manipulate magnetization switching, stimulate magnetization oscillation, and drive domain wall motion in the applications of various spintronic devices. However, magnetization damping as an effective magnetic field is usually ignored in magnetization switching measured by magnetic hysteresis loops due to its dynamical and instantaneous feature. Here, we demonstrate that in addition to the dampinglike SOT effective field, the perpendicular effective field measured by the shift of Hall magnetic hysteresis curves also contains the z-direction effective fields originating from magnetization damping under the total static magnetic field. These findings provide key insights for understanding the effective magnetic fields originated from the magnetic damping and dampinglike SOT effective field in chiral domain walls, and pave the path to practical application of the chiral domain wall systems.

DOI: 10.1103/PhysRevB.107.104411

I. INTRODUCTION

The effective magnetic fields induced by spin-orbit torque (SOT), Dzyaloshinsky-Moriya exchange interaction (DMI), and magnetization damping in chiral domain walls (DWs) play an important role in spintronics. For example, SOT effects have become a hot issue in spintronics due to the emerging applications in switching magnetization of ferromagnets [1], magnetic tunneling junctions [2], antiferromagnetic metals [3], and compensated ferrimagnets [4], manipulating chiral-spin rotation [5] and exchange bias [6], sensing magnetic field [7], inducing domain nucleation [8], driving spin wave propagation [9], and stimulating nano-oscillator [10]. Magnetic damping can also influence the performance of spintronic devices including hard drives, magnetic random-access memories, magnetic logic devices, and magnetic field sensors, since it can determine magnetization relaxation and dissipation [11,12], spin diffusion and pumping [13,14], and spin wave propagation [15].

In order to quantify the SOT effective magnetic field in a perpendicular magnetization film, one of the common methods is to measure the shift of out-of-plane anomalous Hall effect curves by varying the magnetic field along the z axis under the fixed in-plane external field and applied electric current. In chiral ferromagnetic DWs [16], the SOT effective field depends on the in-plane external field and applied electric current used in the measurements. So far, many works have reported that the SOT field increases linearly with the in-plane external magnetic field until saturation [17–20], and the external field at saturation is used to quantitatively estimate the DMI effective field of the chiral ferromagnet. In this case, it is usually believed that the effective field measured by the shift of Hall curve is the dampinglike SOT effective field, but the contribution of magnetization damping under the total static magnetic field has not been considered. In fact, although a lot of work has been carried out on the magnetization damping, magnetization damping as an effective magnetic field is usually ignored in the magnetization switching measured by magnetic hysteresis loops due to its dynamical and instantaneous feature. In addition, the contribution of DW pinning field in the in-plane x-axis direction to the perpendicular effective field in the z-axis direction through magnetization damping has not been noticed in the context of DW motion driven by magnetic field and spin transfer torque [21–25].

In this paper, we studied the relationship between the measured effective field H_z^{eff} in perpendicular direction and the external field H_x in the longitudinal direction of the perpendicularly magnetized single CoPt film. The experimental results and theoretical calculations reveal that H_z^{eff} varies nonlinearly and nonmonotonically with H_x, and the magnetization damping as well as the dampinglike SOT effective field play an important role in the determination of H_z^{eff}. Especially, the good agreement between theory and experiment further demonstrates the effect of DW pinning field H^{pin} on the effective field H_z^{eff} through magnetization damping.

*These authors contributed equally to this paper.
†shishenyan@sdu.edu.cn
‡yftian@sdu.edu.cn

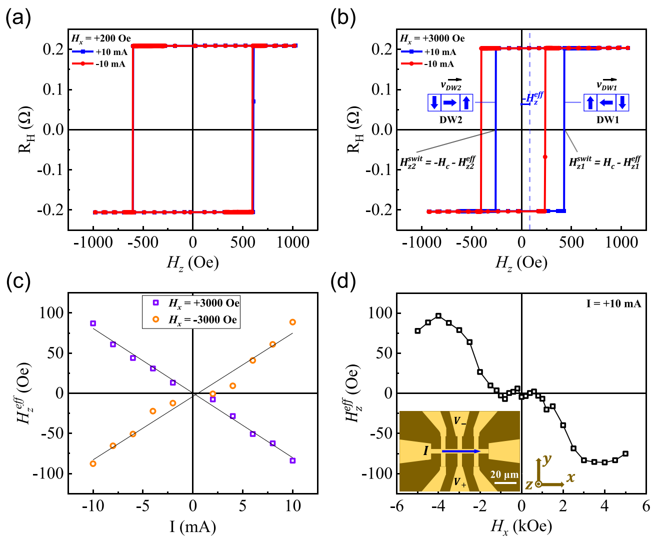

FIG. 1. The out-of-plane anomalous Hall effect curves measured under $H_x = +200$ Oe (a) and $H_x = +3000$ Oe (b) for the applied current $I = \pm 10$ mA in the CoPt ferromagnetic film. The measured z-direction effective bias field H_z^{eff}, and the switching fields H_{z1}^{swit} and H_{z2}^{swit} are marked in (b). (c) H_z^{eff} as a function of the applied current I under $H_x = \pm 3000$ Oe. (d) H_z^{eff} as a function of H_x for the applied current $I = +10$ mA. The bottom inset shows the structural diagram of Hall bar.

II. MEASUREMENTS OF ANOMALOUS HALL EFFECT AND z DIRECTION EFFECTIVE FIELD OF THE CoPt FILM

The perpendicularly magnetized ferromagnetic film of CoPt alloy with the structure of substrate-Si-SiO$_2$/Ta2/Pt5/Co0.5/Pt0.3/Co0.5/Ru2 was prepared by sputtering machine (the numbers are the nominal thickness of each layer in unit of nm), and it presents the electric current induced perpendicular magnetization switching by SOT, as shown in Supplemental Material I [26] (see also Refs. [27–29] therein). Figures 1(a) and 1(b) show the out-of-plane anomalous Hall effect curves of CoPt film measured under fixed H_x and I by varying the magnetic field along the z axis. This is the conventional method used to measure the dampinglike SOT effective bias field H_z^{eff} in the z direction, which can be obtained by the switching fields H_{z1}^{swit} and H_{z2}^{swit} as shown in Fig. 1(b): $H_z^{\mathrm{eff}} = -(H_{z1}^{\mathrm{swit}} + H_{z2}^{\mathrm{swit}})/2$. In Figs. 1(a) and 1(b), we can calculate that $H_z^{\mathrm{eff}} = -3$ Oe for $H_x = +200$ Oe and $I = +10$ mA; and $H_z^{\mathrm{eff}} = -84$ Oe for $H_x = +3000$ Oe and $I = +10$ mA.

Figure 1(c) shows the linear variation of H_z^{eff} with I under $H_x = \pm 3000$ Oe, which is consistent with the observation by other groups [1,17–20]. Figure 1(d) shows the variation of H_z^{eff} with H_x at the fixed current $I = +10$ mA. The dependence of H_z^{eff} on H_x shows the following three characteristics: (i) When $0 \leqslant |H_x| \leqslant 1300$ Oe, the value of $|H_z^{\mathrm{eff}}|$ is nearly zero. (ii) When $|H_x| > 1300$ Oe, $|H_z^{\mathrm{eff}}|$ increases with $|H_x|$ significantly and reaches the maximum at $|H_x| = 4000$ Oe. (iii) When $|H_x| > 4000$ Oe, $|H_z^{\mathrm{eff}}|$ begins to decrease with $|H_x|$. The above characteristics are strikingly different from the results previously reported that the SOT field increases linearly with H_x until saturation [17–20].

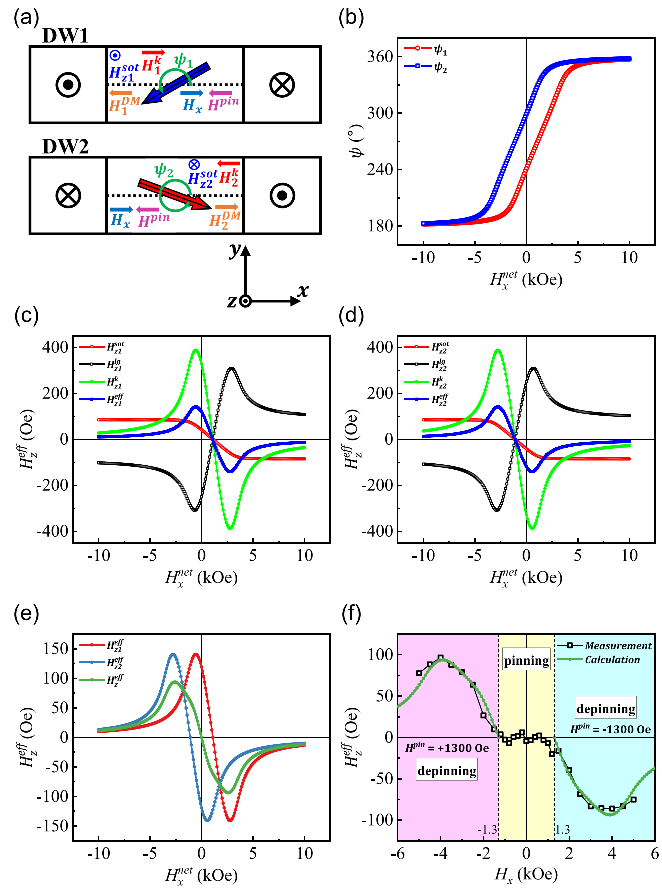

FIG. 2. (a) The schematic diagram of Néel DW with left-handed chirality in the CoPt film. The bottom inset illustrates the directions of x, y, and z axes. The symbols ⊙ and ⊗ represent the magnetic moments in $+\hat{z}$ and $-\hat{z}$ directions. The thicker arrow represents the magnetization vector M_i at the center of the DW, and its azimuth angle with respect to $+\hat{x}$ is represented by ψ_i. The directions of various effective magnetic fields are shown in the center of DW. (b) Theoretical calculations of azimuth angles ψ_1 for DW1 (red) and ψ_2 for DW2 (blue) as a function of net magnetic field H_x^{net} in x direction. (c), (d) Theoretical calculations of z-direction effective bias fields H_{z1}^{eff} for DW1 and H_{z2}^{eff} for DW2 as a function of H_x^{net}. (e) Theoretical calculation of total z-direction effective bias field H_z^{eff} for the multiple domain walls as a function of H_x^{net}. (f) Comparison of measured and calculated H_z^{eff} under different external magnetic field H_x.

III. CALCULATIONS OF z-DIRECTION EFFECTIVE FIELD H_z^{eff} BY DW MODEL

Now we turn to explain the characteristics in Fig. 1(d) by DW dynamics. First, we propose a model of Néel DW with left-handed chirality in Fig. 2(a). The DW of up-to-down is referred to as DW1 in this model and the DW of down-to-up is DW2. Schematically, the magnetization vector at the center of DW is in the x-y plane, and its direction is described by the azimuth angle ψ_i (the subscript $i = 1,\ 2$ for DW1 and DW2, respectively) with respect to $+\hat{x}$. There exist the dampinglike SOT effective field $\boldsymbol{H}_{zi}^{\mathrm{sot}}$, DMI effective field $\boldsymbol{H}_i^{\mathrm{DM}}$, in-plane demagnetization field $\boldsymbol{H}_i^k$ of the domain wall, external magnetic field $\boldsymbol{H}_x$, and corresponding pinning field

$\boldsymbol{H}^{\mathrm{pin}}$, which all act on the magnetization vector at the center of DW. Here, we need to discuss the inevitability of the existence of pinning field $\boldsymbol{H}^{\mathrm{pin}}$. As shown in Fig. 1(b), the effective fields H_{z1}^{eff} and H_{z2}^{eff} satisfy the relationships $H_{z1}^{\mathrm{swit}} = H_c - H_{z1}^{\mathrm{eff}}$ and $H_{z2}^{\mathrm{swit}} = -H_c - H_{z2}^{\mathrm{eff}}$, where H_c is the coercivity of CoPt film. This means that the measurement of z-direction effective field H_{z1}^{eff} (or H_{z2}^{eff}) at the external switching field H_{z1}^{swit} (or H_{z2}^{swit}) is under the critical state of perpendicular magnetization switching. In this state, the DW motion is in the depinning regime rather than the flow regime [23]. Therefore, when the external magnetic field $\boldsymbol{H}_x$ is applied, there is a pinning magnetic field $\boldsymbol{H}^{\mathrm{pin}}$ to counter it [21,22]. The maximum pinning field $|H_{\max}^{\mathrm{pin}}| = 1300$ Oe is evaluated for the as-prepared CoPt film. Only when $|H_x|$ is greater than $|H_{\max}^{\mathrm{pin}}|$, there is a net magnetic field in the x direction $\boldsymbol{H}_x^{\mathrm{net}} = \boldsymbol{H}_x + \boldsymbol{H}^{\mathrm{pin}} \neq 0$ to drive the domain wall movement. Thus, the longitudinal field $\boldsymbol{H}_i^{\mathrm{lg}}$ in the x direction can be defined as $\boldsymbol{H}_i^{\mathrm{lg}} = \boldsymbol{H}_x^{\mathrm{net}} + \boldsymbol{H}_i^{\mathrm{DM}} = \boldsymbol{H}_x + \boldsymbol{H}^{\mathrm{pin}} + \boldsymbol{H}_i^{\mathrm{DM}}$.

Then we consider Landau-Lifshitz-Gilbert (LLG) equation for DW1 and DW2 of the CoPt ferromagnetic film, respectively:

$$\frac{\partial \boldsymbol{M}_i}{\partial t} = -\gamma \boldsymbol{M}_i \times \boldsymbol{H}_i^{\mathrm{stat}} + \frac{\alpha}{M_i}\boldsymbol{M}_i \times \frac{\partial \boldsymbol{M}_i}{\partial t} + \frac{\gamma H_i^{DLy}}{M_i}\boldsymbol{M}_i \times (\boldsymbol{M}_i \times \hat{y}). \quad (1)$$

Here the item of $-\gamma \boldsymbol{M}_i \times \boldsymbol{H}_i^{\mathrm{stat}}$ presents the precession of magnetization $\boldsymbol{M}_i$ at the center of DW under the total static effective magnetic field $\boldsymbol{H}_i^{\mathrm{stat}}$, where γ is gyromagnetic ratio. The item of $\frac{\alpha}{M_i}\boldsymbol{M}_i \times \frac{\partial \boldsymbol{M}_i}{\partial t}$ is the dynamical damping of magnetization $\boldsymbol{M}_i$, where α is the damping factor. And the item of $\frac{\gamma H_i^{DLy}}{M_i}\boldsymbol{M}_i \times (\boldsymbol{M}_i \times \hat{y})$ is the dampinglike SOT term caused by the spin current with polarization in $+\hat{y}$, where H_i^{DLy} is the amplitude of the dampinglike SOT effective field. In Eq. (1), all the static magnetic fields felt by $\boldsymbol{M}_i$ are contained in $\boldsymbol{H}_i^{\mathrm{stat}}$. Specifically, the static effective field $\boldsymbol{H}_i^{\mathrm{stat}}$ is determined by the magnetostatic energy density w_i: $\boldsymbol{H}_i^{\mathrm{stat}} = -\frac{\partial w_i}{\partial \boldsymbol{M}_i} = \boldsymbol{H}_x + \boldsymbol{H}^{\mathrm{pin}} + \boldsymbol{H}_i^{\mathrm{DM}} + \boldsymbol{H}_i^k = \boldsymbol{H}_x^{\mathrm{net}} + \boldsymbol{H}_i^{\mathrm{DM}} + \boldsymbol{H}_i^k = \boldsymbol{H}_i^{\mathrm{lg}} + \boldsymbol{H}_i^k$. Here, different terms in this equation present the external field $\boldsymbol{H}_x = H_x\hat{x}$, pinning field $\boldsymbol{H}^{\mathrm{pin}} = H^{\mathrm{pin}}\hat{x}$, DMI effective field $\boldsymbol{H}_i^{\mathrm{DM}} = H_i^{\mathrm{DM}}\hat{x}$ (where H_i^{DM} is regarded as a constant for each DW), in-plane demagnetization field $\boldsymbol{H}_i^k = -H_i^k \cos\psi_i \hat{x}$ of the domain wall (where $H_i^k = 4\pi M_i N$ is the amplitude of demagnetization field), net magnetic field $\boldsymbol{H}_x^{\mathrm{net}} = H_x^{\mathrm{net}}\hat{x}$, and the longitudinal field $\boldsymbol{H}_i^{\mathrm{lg}} = H_i^{\mathrm{lg}}\hat{x}$. For the demagnetization field $H_i^k = 4\pi M_i N$, N is the demagnetization factor of the domain wall, which can be estimated by the layer thickness d and the DW width Δ: $N \approx \frac{d}{d+\Delta}$. Based on LLG Eq. (1), the equation of static effective field $\boldsymbol{H}_i^{\mathrm{stat}}$, and rigid profile of the one-dimensional DW model [16,30], DW dynamics of the CoPt film can be completely described by the DW velocity and the DW azimuth angle ψ_i (see Supplemental Material II for the calculation method [26]).

By using the parameters $\alpha = 0.26$, $H_1^{\mathrm{DM}} = -1100$ Oe, $H_2^{\mathrm{DM}} = +1100$ Oe, $H_1^k = H_2^k = 2981$ Oe, and $H_1^{DLy} = H_2^{DLy} = 85$ Oe (see Supplemental Material III and Table S1 for details of the physical parameters [26]), the azimuth angles ψ_1 of DW1 and ψ_2 of DW2 as a function of net magnetic field H_x^{net} are calculated as shown in Fig. 2(b). Utilizing ψ_1 and ψ_2 of DW1 and DW2, we can theoretically reproduce the relationship between z-direction effective bias field H_z^{eff} and external field H_x in Fig. 1(d) to clarify the physical origin of H_z^{eff}.

The key is to check whether $\boldsymbol{H}_z^{\mathrm{eff}}$ contains others effective fields in the z direction besides dampinglike SOT effective field $\boldsymbol{H}_{zi}^{\mathrm{sot}}$. Skillfully, the LLG Eq. (1) can be transformed into another form by using $\gamma = \gamma'(1+\alpha^2)$ [31]:

$$\frac{\partial \boldsymbol{M}_i}{\partial t} = -\gamma' \boldsymbol{M}_i \times \boldsymbol{H}_i^{\mathrm{stat}} - \frac{\alpha\gamma'}{M_i}\boldsymbol{M}_i \times \left(\boldsymbol{M}_i \times \boldsymbol{H}_i^{\mathrm{stat}}\right) - \left(\gamma'\alpha H_i^{DLy}\right)\boldsymbol{M}_i \times \hat{y} + \frac{\gamma' H_i^{DLy}}{M_i}\boldsymbol{M}_i \times (\boldsymbol{M}_i \times \hat{y}). \quad (2)$$

Since $\alpha^2 \ll 1$, we can regard $\gamma' \approx \gamma$ in Eq. (2). It can be found by comparison that the dynamical damping $\frac{\alpha}{M_i}\boldsymbol{M}_i \times \frac{\partial \boldsymbol{M}_i}{\partial t}$ in Eq. (1) is converted into $-\frac{\alpha\gamma'}{M_i}\boldsymbol{M}_i \times (\boldsymbol{M}_i \times \boldsymbol{H}_i^{\mathrm{stat}})$. For $\boldsymbol{m}_i = \frac{\boldsymbol{M}_i}{M_i}$, we can see that $\boldsymbol{m}_i \times \alpha\boldsymbol{H}_i^{\mathrm{stat}}$ and $\boldsymbol{m}_i \times (-H_i^{DLy}\hat{y})$ represent two damping effective magnetic fields. For the Néel DW in Fig. 2(a), the $\boldsymbol{m}_i$ at the center of the DW is in the x-y plane, so both fields are in the z direction.

The form of the z-direction effective field $\boldsymbol{m}_i \times \alpha\boldsymbol{H}_i^{\mathrm{stat}}$ can be further separated: $\boldsymbol{m}_i \times \alpha\boldsymbol{H}_i^{\mathrm{stat}} = \boldsymbol{m}_i \times \alpha\boldsymbol{H}_i^{lg} + \boldsymbol{m}_i \times \alpha\boldsymbol{H}_i^k$. We define $\boldsymbol{H}_{zi}^{lg}$ and $\boldsymbol{H}_{zi}^k$ as z-direction effective fields caused by $\boldsymbol{H}_i^{\mathrm{lg}}$ and $\boldsymbol{H}_i^k$ respectively:

$$\boldsymbol{H}_{zi}^{\mathrm{lg}} = \boldsymbol{m}_i \times \alpha\boldsymbol{H}_i^{\mathrm{lg}} = \alpha H_i^{\mathrm{lg}}(-\sin\psi_i)\hat{z}, \quad (3)$$

$$\boldsymbol{H}_{zi}^k = \boldsymbol{m}_i \times \alpha\boldsymbol{H}_i^k = \alpha H_i^k(\sin\psi_i\cos\psi_i)\hat{z}, \quad (4)$$

and the dampinglike SOT effective field is described as

$$\boldsymbol{H}_{zi}^{\mathrm{sot}} = \boldsymbol{m}_i \times \left(-H_i^{DLy}\hat{y}\right) = \left(-H_i^{DLy}\right)\cos\psi_i\hat{z}. \quad (5)$$

Thus, Eqs. (3)–(5) represent all z-direction effective fields acting on the DWs. More specifically, the z-direction effective fields $\boldsymbol{H}_{z1}^{\mathrm{eff}}$ of DW1 and $\boldsymbol{H}_{z2}^{\mathrm{eff}}$ of DW2 are $\boldsymbol{H}_{z1}^{\mathrm{eff}} = \boldsymbol{H}_{z1}^{\mathrm{lg}} + \boldsymbol{H}_{z1}^k + \boldsymbol{H}_{z1}^{\mathrm{sot}}$ and $\boldsymbol{H}_{z2}^{\mathrm{eff}} = \boldsymbol{H}_{z2}^{\mathrm{lg}} + \boldsymbol{H}_{z2}^k + \boldsymbol{H}_{z2}^{\mathrm{sot}}$, respectively. Consequently, the total z-direction effective bias field $\boldsymbol{H}_z^{\mathrm{eff}}$ of the multiple domain walls is the average of $\boldsymbol{H}_{z1}^{\mathrm{eff}}$ and $\boldsymbol{H}_{z2}^{\mathrm{eff}}$: $\boldsymbol{H}_z^{\mathrm{eff}} = (\boldsymbol{H}_{z1}^{\mathrm{eff}} + \boldsymbol{H}_{z2}^{\mathrm{eff}})/2 = -(\boldsymbol{H}_{z1}^{\mathrm{swit}} + \boldsymbol{H}_{z2}^{\mathrm{swit}})/2$ (see Supplemental Material IV for the demonstration of the equation [26]). From this equation, we can see that the theoretical and experimental $\boldsymbol{H}_z^{\mathrm{eff}}$ are calculated in the same way.

By using the azimuth angles ψ_i under different net magnetic field H_x^{net} in Fig. 2(b) and Eqs. (3)–(5), we can get all the z-direction effective fields $\boldsymbol{H}_{z1}^{\mathrm{lg}}$, $\boldsymbol{H}_{z1}^k$, $\boldsymbol{H}_{z1}^{\mathrm{sot}}$, and $\boldsymbol{H}_{z1}^{\mathrm{eff}}$ under different $\boldsymbol{H}_x^{\mathrm{net}}$ for DW1 as shown in Fig. 2(c). Apparently, when $H_x^{\mathrm{net}} = -H_1^{\mathrm{DM}} = +1100$ Oe, $\boldsymbol{H}_{z1}^{\mathrm{lg}}$, $\boldsymbol{H}_{z1}^k$, $\boldsymbol{H}_{z1}^{\mathrm{sot}}$, and $\boldsymbol{H}_{z1}^{\mathrm{eff}}$ are all zero, which are caused by $H_1^{\mathrm{lg}} = 0$ and $\psi_1 = 270^\circ$ [shown in Fig. 2(b)]. Furthermore, it can be seen that the four curves of $\boldsymbol{H}_{z1}^{\mathrm{lg}}$, $\boldsymbol{H}_{z1}^k$, $\boldsymbol{H}_{z1}^{\mathrm{sot}}$ and $\boldsymbol{H}_{z1}^{\mathrm{eff}}$ varying with $\boldsymbol{H}_x^{\mathrm{net}}$ are inversion symmetrical about the point of $H_x^{\mathrm{net}} = +1100$ Oe. For the dampinglike SOT effective field $\boldsymbol{H}_{z1}^{\mathrm{sot}}$, its magnitude increases approximately linearly with $\boldsymbol{H}_x^{\mathrm{net}}$ until it tends to saturation.

Dramatically, $\boldsymbol{H}_{z1}^{\mathrm{lg}}$ and $\boldsymbol{H}_{z1}^{k}$ show opposite trends and partially cancel out the $\boldsymbol{H}_{z1}^{\mathrm{eff}}$. Adding up the three curves of $\boldsymbol{H}_{z1}^{\mathrm{lg}}$, $\boldsymbol{H}_{z1}^{k}$, and $\boldsymbol{H}_{z1}^{\mathrm{sot}}$, the curve of $\boldsymbol{H}_{z1}^{\mathrm{eff}}$ is obtained, which represents the z-direction effective field acting on DW1 under different $\boldsymbol{H}_{x}^{\mathrm{net}}$. In the same way, z-direction effective fields $\boldsymbol{H}_{z2}^{\mathrm{lg}}$, $\boldsymbol{H}_{z2}^{k}$, $\boldsymbol{H}_{z2}^{\mathrm{sot}}$, and $\boldsymbol{H}_{z2}^{\mathrm{eff}}$ under different $\boldsymbol{H}_{x}^{\mathrm{net}}$ for DW2 can be calculated as shown in Fig. 2(d). Finally, the total z-direction effective bias field $\boldsymbol{H}_{z}^{\mathrm{eff}}$ of the multiple domain walls under different $\boldsymbol{H}_{x}^{\mathrm{net}}$ is shown in Fig. 2(e). Considering $\boldsymbol{H}_{x}^{\mathrm{net}} = \boldsymbol{H}_x + \boldsymbol{H}^{\mathrm{pin}}$ and typical features of $\boldsymbol{H}^{\mathrm{pin}}$, we can obtain the relationship between $\boldsymbol{H}_{z}^{\mathrm{eff}}$ and $\boldsymbol{H}_x$ from Fig. 2(e), as shown in Fig. 2(f). By comparing the calculation and experimental results in Fig. 2(f), we can clarify the variation of the z-direction effective bias field $\boldsymbol{H}_{z}^{\mathrm{eff}}$ with external field $\boldsymbol{H}_x$: when $|H_x| \leqslant H_{\max}^{\mathrm{pin}}$, $\boldsymbol{H}_{z}^{\mathrm{eff}}$ is zero; and when $|H_x| > H_{\max}^{\mathrm{pin}}$, $\boldsymbol{H}_{z}^{\mathrm{eff}}$ is determined by the dampinglike SOT effective field $\boldsymbol{H}_{zi}^{\mathrm{sot}}$ and the other two z-direction effective fields $\boldsymbol{H}_{zi}^{\mathrm{lg}}$ and $\boldsymbol{H}_{zi}^{k}$ which are caused by the dynamical damping. We also calculated the hysteresis loops and effective magnetic field H_z^{eff} corresponding to those in Figs. 1(a), 1(b), and 1(d) by micromagnetic simulation (see Supplemental Material V for detailed results [26]). The results of micromagnetic simulation are quite consistent with the experimental measurements, which proves the correctness of our theoretical DW model and the rationality of our calculation method used in Fig 2.

IV. MEASUREMENTS AND CALCULATIONS OF z-DIRECTION EFFECTIVE FIELD OF THE ANNEALED CoPt FILM

Furthermore, we apply a high electric current pulse with intensity of 40 mA and duration of 0.1 s twice to anneal the CoPt ferromagnetic film and reduce the pinning field. For the annealed CoPt film by electric current pulses, the shift of out-of-plane anomalous Hall effect curves under the fixed H_x and I is shown in Figs. 3(a) and 3(b). In Figs. 3(a) and 3(b), we can calculate $H_z^{\mathrm{eff}} = -17$ Oe for $H_x = +200$ Oe and $I = +10$ mA, and $H_z^{\mathrm{eff}} = -84$ Oe for $H_x = +3000$ Oe and $I = +10$ mA. Keeping $I = +10$ mA and scanning H_x, the variation of H_z^{eff} with H_x is shown in Fig. 3(c). It is clear that the magnitude of H_z^{eff} increases linearly with H_x until saturation, which is similar to the results previously reported [17–20].

The linear dependence of H_z^{eff} on H_x can also be explained within the same theoretical framework of DW dynamics. After annealing, the defects are greatly reduced and the pinning field can be neglected. Therefore, we simplify the DW model as follows: $\boldsymbol{H}_i^{k}$ completely cancels $\boldsymbol{H}_i^{\mathrm{lg}}$ within a certain range, i.e.,

$$\boldsymbol{H}_i^{\mathrm{stat}} = H_x + H_i^{\mathrm{DM}} - H_i^{k}\cos\psi_i = 0. \tag{6}$$

Hence we get $\cos\psi_i = (H_x + H_i^{\mathrm{DM}})/H_i^{k}$, when $-H_i^{k} - H_i^{\mathrm{DM}} \leqslant H_x \leqslant H_i^{k} - H_i^{\mathrm{DM}}$. It is clear that the DW azimuth angles ψ_i tends to be 0° or 180° when $H_x > H_i^{k} - H_i^{\mathrm{DM}}$ or $H_x < -H_i^{k} - H_i^{\mathrm{DM}}$. Combining Eqs. (5) and (6), we can obtain $\boldsymbol{H}_{zi}^{\mathrm{sot}} = -\frac{H_i^{DLy}}{H_i^{k}}(H_x + H_i^{\mathrm{DM}})\hat{z}$. This is the linear dependence between the SOT effective field $\boldsymbol{H}_{zi}^{\mathrm{sot}}$ and the external in-plane field H_x. In the case of $\boldsymbol{H}_i^{\mathrm{stat}} = 0$, there is only the dampinglike SOT effective field $\boldsymbol{H}_{zi}^{\mathrm{sot}}$ in the z direction in Eq. (2). Thus, the total effective field $\boldsymbol{H}_z^{\mathrm{eff}}$ changes to $\boldsymbol{H}_z^{\mathrm{eff}} = (\boldsymbol{H}_{z1}^{\mathrm{sot}} + \boldsymbol{H}_{z2}^{\mathrm{sot}})/2$.

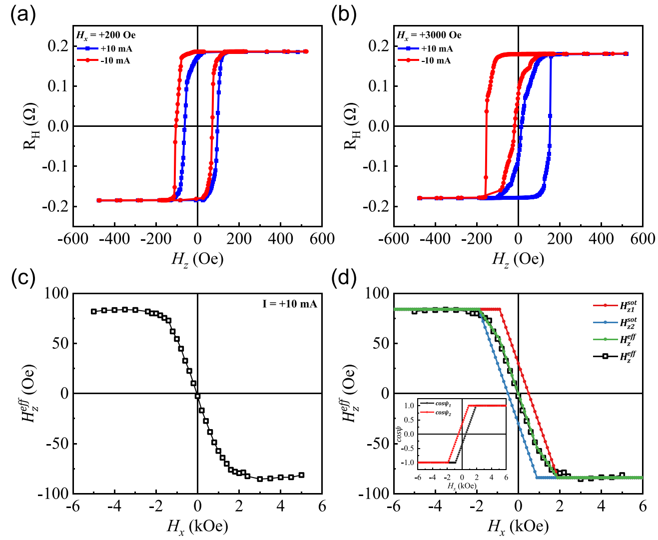

FIG. 3. The out-of-plane anomalous Hall effect curves measured under $H_x = +200$ Oe (a) and $H_x = +3000$ Oe (b) for $I = \pm 10$ mA in the annealed CoPt film. (c) The measured z-direction effective bias field H_z^{eff} versus H_x for $I = +10$ mA in the annealed CoPt film. (d) Theoretical calculations of dampinglike SOT effective fields H_{z1}^{sot} (red) in DW1, H_{z2}^{sot} (blue) in DW2, and total z-direction effective bias field H_z^{eff} (green) as a function of H_x. The comparison of measured (black) and calculated (green) H_z^{eff} for the annealed CoPt film is highlighted. The inset shows the relationship between $\cos\psi_1$, $\cos\psi_2$, and H_x in the calculations.

Due to the annealing effect, the coercivity H_c, DMI effective field $\boldsymbol{H}_i^{\mathrm{DM}}$, and demagnetization field $\boldsymbol{H}_i^{k}$ of the CoPt film all reduce significantly. Substituting the parameters $H_1^{\mathrm{DM}} = -500$ Oe, $H_2^{\mathrm{DM}} = +500$ Oe, and $H_1^{k} = H_2^{k} = 1400$ Oe into Eq. (6), we can get the variation of $\cos\psi_1$ and $\cos\psi_2$ with H_x as shown in the inset of Fig. 3(d). It is worth pointing out that when $H_x = -H_1^{\mathrm{DM}} = +500$ Oe, we obtain $\cos\psi_1 = 0$ for DW1, and when $H_x = -H_2^{\mathrm{DM}} = -500$ Oe, we obtain $\cos\psi_2 = 0$ for DW2. This means that when $\boldsymbol{H}_x$ and $\boldsymbol{H}_i^{\mathrm{DM}}$ completely cancel out, the Néel DWs transform into the Bloch DWs, corresponding to DW azimuth angle $\psi_i = 90^\circ$ or 270°. By using $H_1^{DLy} = H_2^{DLy} = 85$ Oe, and the values of $\cos\psi_1$ and $\cos\psi_2$ at different H_x in Eq. (6), $\boldsymbol{H}_{z1}^{\mathrm{sot}}$ and $\boldsymbol{H}_{z2}^{\mathrm{sot}}$ in Eq. (5) can be calculated under different $\boldsymbol{H}_x$ as shown in Fig. 3(d), and then the total z-direction effective bias field $\boldsymbol{H}_z^{\mathrm{eff}}$ for the multiple domain walls is obtained. Obviously, when $H_x = H_1^{k} - H_1^{\mathrm{DM}}$ and $H_x = -H_2^{k} - H_2^{\mathrm{DM}}$, the effective field $\boldsymbol{H}_z^{\mathrm{eff}}$ reaches saturation value, rather than $H_x = -H_1^{\mathrm{DM}}$ or $H_x = -H_2^{\mathrm{DM}}$ as commonly stated.

V. CONCLUSIONS

In conclusion, the experimental results and theoretical calculations demonstrate that the effective field measured by the shift of Hall curves includes not only the dampinglike SOT field, but also other z-direction effective fields in the form of dynamical damping, which are caused by the external magnetic field, pinning field, DMI effective field, and in-plane demagnetization field. Only when the total static effective field $\boldsymbol{H}_i^{\mathrm{stat}}$ becomes zero is the effective field measured by the shift of Hall curves exactly equal to the dampinglike SOT field.

ACKNOWLEDGMENTS

This work was supported by the National Natural Science Foundation of China (Grants No. 51871112, No. 12174219, and No. 11774199), the 111 Project B13029, and the Major Basic Research Project of Shandong Province (Grant No. ZR2020ZD28).

[1] X. Xie, X. Zhao, Y. Dong, X. Qu, K. Zheng, X. Han, X. Han, Y. Fan, L. Bai, Y. Chen, Y. Dai, Y. Tian, and S. Yan, Controllable field-free switching of perpendicular magnetization through bulk spin-orbit torque in symmetry-broken ferromagnetic films, Nat. Commun. **12**, 2473 (2021).

[2] E. Grimaldi, V. Krizakova, G. Sala, F. Yasin, S. Couet, G. S. Kar, K. Garello, and P. Gambardella, Single-shot dynamics of spin–orbit torque and spin transfer torque switching in three-terminal magnetic tunnel junctions, Nat. Nanotechnol. **15**, 111 (2020).

[3] S. Dutta Gupta, A. Kurenkov, O. A. Tretiakov, G. Krishnaswamy, G. Sala, V. Krizakova, F. Maccherozzi, S. S. Dhesi, P. Gambardella, S. Fukami *et al.*, Spin-orbit torque switching of an antiferromagnetic metallic heterostructure, Nat. Commun. **11**, 5715 (2020).

[4] H. Wu, Y. Xu, P. Deng, Q. Pan, S. A. Razavi, K. Wong, L. Huang, B. Dai, Q. Shao, G. Yu *et al.*, Spin-orbit torque switching of a nearly compensated ferrimagnet by topological surface states, Adv. Mater. **31**, 1901681 (2019).

[5] Y. Takeuchi, Y. Yamane, J.-Y. Yoon, R. Itoh, B. Jinnai, S. Kanai, J. Ieda, S. Fukami, and H. Ohno, Chiral-spin rotation of non-collinear antiferromagnet by spin–orbit torque, Nat. Mater. **20**, 1364 (2021).

[6] P.-H. Lin, B.-Y. Yang, M.-H. Tsai, P.-C. Chen, K.-F. Huang, H.-H. Lin, and C.-H. Lai, Manipulating exchange bias by spin–orbit torque, Nat. Mater. **18**, 335 (2019).

[7] R. Li, S. Zhang, S. Luo, Z. Guo, Y. Xu, J. Ouyang, M. Song, Q. Zou, L. Xi, X. Yang *et al.*, A spin–orbit torque device for sensing three-dimensional magnetic fields, Nat. Electron. **4**, 179 (2021).

[8] J. Zhou, T. Zhao, X. Shu, L. Liu, W. Lin, S. Chen, S. Shi, X. Yan, X. Liu, and J. Chen, Spin–orbit torque-induced domain nucleation for neuromorphic computing, Adv. Mater. **33**, 2103672 (2021).

[9] H. Fulara, M. Zahedinejad, R. Khymyn, A. A. Awad, S. Muralidhar, M. Dvornik, and J. Åkerman, Spin-orbit torque–driven propagating spin waves, Sci. Adv. **5**, eaax8467 (2019).

[10] M. Haidar, A. A. Awad, M. Dvornik, R. Khymyn, A. Houshang, and J. Åkerman, A single layer spin-orbit torque nano-oscillator, Nat. Commun. **10**, 2362 (2019).

[11] L. Chen, S. Mankovsky, S. Wimmer, M. A. W. Schoen, H. S. Körner, M. Kronseder, D. Schuh, D. Bougeard, H. Ebert, D. Weiss *et al.*, Emergence of anisotropic Gilbert damping in ultrathin Fe layers on GaAs(001), Nat. Phys. **14**, 490 (2018).

[12] K. M. D. Hals and A. Brataas, Magnetization dissipation in the ferromagnetic semiconductor (Ga,Mn)As, Phys. Rev. B **84**, 104404 (2011).

[13] H. Wang, J. Chen, T. Liu, J. Zhang, K. Baumgaertl, C. Guo, Y. Li, C. Liu, P. Che, S. Tu *et al.*, Chiral Spin-Wave Velocities Induced by All-Garnet Interfacial Dzyaloshinskii-Moriya Interaction in Ultrathin Yttrium Iron Garnet Films, Phys. Rev. Lett. **124**, 027203 (2020).

[14] J.-C. Rojas-Sánchez, N. Reyren, P. Laczkowski, W. Savero, J.-P. Attané, C. Deranlot, M. Jamet, J.-M. George, L. Vila, and H. Jaffrès, Spin Pumping and Inverse Spin Hall Effect in Platinum: The Essential Role of Spin-Memory Loss at Metallic Interfaces, Phys. Rev. Lett. **112**, 106602 (2014).

[15] H. L. Wang, C. H. Du, Y. Pu, R. Adur, P. C. Hammel, and F. Y. Yang, Scaling of Spin Hall Angle in 3d, 4d, and 5d Metals from $Y_3Fe_5O_{12}$/Metal Spin Pumping, Phys. Rev. Lett. **112**, 197201 (2014).

[16] S. Emori, U. Bauer, S.-M. Ahn, E. Martinez, and G. S. D. Beach, Current-driven dynamics of chiral ferromagnetic domain walls, Nat. Mater. **12**, 611 (2013).

[17] C.-F. Pai, M. Mann, A.-J. Tan, and G. S. D. Beach, Determination of spin torque efficiencies in heterostructures with perpendicular magnetic anisotropy, Phys. Rev. B **93**, 144409 (2016).

[18] J. Finley and L. Liu, Spin-Orbit-Torque Efficiency in Compensated Ferrimagnetic Cobalt-Terbium Alloys, Phys. Rev. Appl. **6**, 054001 (2016).

[19] J. Han, A. Richardella, S. A. Siddiqui, J. Finley, N. Samarth, and L. Liu, Room-Temperature Spin-Orbit Torque Switching Induced by a Topological Insulator, Phys. Rev. Lett. **119**, 077702 (2017).

[20] Y. Ishikuro, M. Kawaguchi, N. Kato, Y.-C. Lau, and M. Hayashi, Dzyaloshinskii-Moriya interaction and spin-orbit torque at the Ir/Co interface, Phys. Rev. B **99**, 134421 (2019).

[21] M. Hayashi, L. Thomas, Y. B. Bazaliy, C. Rettner, R. Moriya, X. Jiang, and S. S. P. Parkin, Influence of Current on Field-Driven Domain Wall Motion in Permalloy Nanowires from Time Resolved Measurements of Anisotropic Magnetoresistance, Phys. Rev. Lett. **96**, 197207 (2006).

[22] G. S. D. Beach, C. Knutson, C. Nistor, M. Tsoi, and J. L. Erskine, Nonlinear Domain-Wall Velocity Enhancement by Spin-Polarized Electric Current, Phys. Rev. Lett. **97**, 057203 (2006).

[23] P. J. Metaxas, J. P. Jamet, A. Mougin, M. Cormier, J. Ferré, V. Baltz, B. Rodmacq, B. Dieny, and R. L. Stamps, Creep and Flow Regimes of Magnetic Domain-Wall Motion in Ultrathin Pt/Co/Pt Films with Perpendicular Anisotropy, Phys. Rev. Lett. **99**, 217208 (2007).

[24] L. S. E. Alvarez, K.-Y. Wang, S. Lepadatu, S. Landi, S. J. Bending, and C. H. Marrows, Spin-Transfer-Torque-Assisted Domain-Wall Creep in a Co/Pt Multilayer Wire, Phys. Rev. Lett. **104**, 137205 (2010).

[25] D. Chiba, M. Kawaguchi, S. Fukami, N. Ishiwata, K. Shimamura, K. Kobayashi, and T. Ono, Electric-field control of magnetic domain-wall velocity in ultrathin cobalt with perpendicular magnetization, Nat. Commun. **3**, 888 (2012).

[26] See Supplemental Material at http://link.aps.org/supplemental/10.1103/PhysRevB.107.104411 for the details of more experimental and theoretical results.

[27] A. P. Malozemoff and J. C. Slonczewski, *Magnetic Domain Walls in Bubble Materials* (Academic, New York, 1979).

[28] S. Zhang and Z. Li, Roles of Nonequilibrium Conduction Electrons on the Magnetization Dynamics of Ferromagnets, Phys. Rev. Lett. **93**, 127204 (2004).

[29] A. Thiaville, Y. Nakatani, J. Miltat, and Y. Suzuki, Micromagnetic understanding of current-driven domain wall motion in patterned nanowires, Europhys. Lett. **69**, 990 (2005).

[30] S.-H. Yang, K.-S. Ryu, and S. Parkin, Domain-wall velocities of up to $750\,\mathrm{m\,s^{-1}}$ driven by exchange-coupling torque in synthetic antiferromagnets, Nat. Nanotechnol. **10**, 221 (2015).

[31] F. Hellman, A. Hoffmann, Y. Tserkovnyak, G. S. D. Beach, E. E. Fullerton, C. Leighton, A. H. MacDonald, D. C. Ralph, D. A. Arena, H. A. Dürr *et al.*, Interface-induced phenomena in magnetism, Rev. Mod. Phys. **89**, 025006 (2017).